




Article

# Amino Acid Replacement at Position 228 Induces Fluctuation in the $\Omega$ -Loop of KPC-3 and Reduces the Affinity against Oxyimino Cephalosporins: Kinetic and Molecular Dynamics Studies

Alessandra Piccirilli <sup>1,\*</sup>, Fabrizia Brisdelli <sup>1</sup>, Jean Denis Docquier <sup>2</sup> , Massimiliano Aschi <sup>3</sup>, Sabrina Cherubini <sup>1</sup>, Filomena De Luca <sup>2</sup>, André Matagne <sup>4</sup> , Gianfranco Amicosante <sup>1</sup> and Mariagrazia Perilli <sup>1</sup> 

<sup>1</sup> Dipartimento di Scienze Cliniche Applicate e Biotecnologiche, Università degli Studi dell'Aquila, I-67100 L'Aquila, Italy; fabrizia.brisdelli@univaq.it (F.B.); sabrina.cherubini@graduate.univaq.it (S.C.); gianfranco.amicosante@univaq.it (G.A.); mariagrazia.perilli@univaq.it (M.P.)

<sup>2</sup> Dipartimento di Biotecnologie Mediche, Università di Siena, I-53100 Siena, Italy; jddocquier@unisi.it (J.D.D.); deluca19@unisi.it (F.D.L.)

<sup>3</sup> Dipartimento di Scienze Fisiche e Chimiche, Università degli Studi dell'Aquila, I-67100 L'Aquila, Italy; massimiliano.aschi@univaq.it

<sup>4</sup> Laboratoire d'Enzymologie et Repliement des Protéines, Centre d'Ingénierie des Protéines, Université de Liège, Allée du 6 Août B6c, Sart-Tilman, 4000 Liège, Belgium; amatagne@uliege.be

\* Correspondence: alessandra.piccirilli@univaq.it; Tel.: +39-0862-433489

Received: 9 November 2020; Accepted: 11 December 2020; Published: 16 December 2020



**Abstract:** KPC enzymes are the most common class A carbapenemases globally diffused. The peculiarity of this family of  $\beta$ -lactamases is represented by their ability to hydrolyse all classes of  $\beta$ -lactams, including carbapenems, posing a serious problem to public health. In the present study, seven laboratory mutants of KPC-3 (D228S, D228W, D228M, D228K, D228L, D228I and D228G) were generated by site-saturation mutagenesis to explore the role of residue 228, a non-active site residue. Compared to KPC-3, the seven mutants showed evident differences in  $k_{cat}$  and  $K_m$  values calculated for some penicillins, cephalosporins and carbapenems. In particular, D228S and D228M showed a significant increase of  $K_m$  values for cefotaxime and ceftazidime. Circular dichroism (CD) experiments have demonstrated that substitution at position 228 does not affect the secondary structure of the mutants. Molecular dynamics (MD) simulations were performed on KPC-3, D228S and D228M uncomplexed and complexed with cefotaxime (substrate). Although the residue 228 is located far from the active site, between  $\alpha 11$  helix and  $\beta 7$  sheet in the opposite site of the  $\Omega$ -loop, amino acid substitution at this position generates mechanical effects in the active site resulting in enzyme activity changes.

**Keywords:** beta-lactamases; KPC carbapenemase; kinetic analysis; molecular dynamics

## 1. Introduction

$\beta$ -Lactamases are bacterial enzymes that efficiently hydrolyse  $\beta$ -lactam antibiotics, the most common antimicrobials used in clinical therapy [1]. On the basis of catalytic mechanism,  $\beta$ -lactamases include two distinct groups: serine  $\beta$ -lactamases (SBLs), which hydrolyse  $\beta$ -lactams via a catalytic serine, and metallo- $\beta$ -lactamases (MBLs), which need one or two essential zinc ions for catalysis [2,3]. According to Ambler classification,  $\beta$ -lactamases are categorized into four molecular classes (A, B, C and D) based on primary amino acid similarities [4]. To date, about 3000 different  $\beta$ -lactamases have been identified in

natural bacterial isolates, and a functional classification scheme is currently used that takes into account substrate and inhibitor profiles [5]. The class B zinc-dependent  $\beta$ -lactamases are metallo-enzymes which are able to hydrolyse the amide bond of  $\beta$ -lactam ring of most  $\beta$ -lactams, especially carbapenems. On the basis of sequence homologies, three distinct MBL superfamilies have been identified: subclasses B1 and B3, which work with two zinc ions, and subclass B2, with one zinc ion [6]. The most widespread  $\beta$ -lactamases are the enzymes belonging to molecular class A, which include  $\beta$ -lactamases with an extended spectrum of substrates (named ESBLs), and carbapenemases, able to hydrolyse carbapenems, the “antibiotics of last resort” [7].

Class A  $\beta$ -lactamases are globular proteins with two structural domains,  $\alpha$  and  $\alpha/\beta$  domains, and the active site is situated in a groove between these two domains. Several conserved amino acids in the active site appear to be directly or indirectly involved in the substrate recognition and catalysis. In the catalytic mechanism of class A  $\beta$ -lactamases, a crucial role is played by serine 70 (S70), involving acylation and deacylation steps [8]. The mechanism of catalysis is based on the presence of a proton pump in the catalytic pocket represented by three residues: K73, S130 and E166. Molecular modelling studies have identified a conserved water molecule which might act as a relay molecule in the transfer of the proton between the S70 and E166 side chains. Residue E166 is part of a structural element called  $\Omega$ -loop, which is a mobile and flexible structure making it possible to reduce the distance between the two residues during the acylation process [8]. In the present study, we focused our attention on KPC  $\beta$ -lactamase, which, in *Enterobacteriales* clinical strains, confers resistance to extended spectrum  $\beta$ -lactams, including carbapenems.

Specifically, carbapenem-resistant *Enterobacteriales* have emerged globally and may produce either KPC-type variants (class A), OXA-48-derived variants (class D), or class B metallo- $\beta$ -lactamases (e.g., IMP-, VIM- or NDM-type variants) [3]. The global spread of KPC enzyme is due to the fact that *bla*<sub>KPC</sub> genes are located in mobile genetic elements. In fact, the *bla*<sub>KPC</sub> genes have been reported on different plasmid types, such as IncF, IncFII(K1), IncR, IncX, IncX3, IncI2, ColE1 incompatibility group plasmids, and are associated with transposon related structure (i.e., Tn4401), including *trpR*, *trpA*, *ISKpn6* and *ISKpn7* elements [9–13]. In most cases, the aforementioned plasmids harbour genes conferring resistance to other classes of antibiotics, such as aminoglycosides, fluoroquinolones, tetracyclines, sulphonamides making infections caused by KPC-producing isolates difficult to treat. To date, more than fifty KPC variants have been reported (<http://www.ncbi.nlm.nih.gov/pathogens/isolates#/refgene/KPC>, data version 31 October 2020). However, KPC-2 and KPC-3 remain the most widespread globally [14]. The KPC-3 differs by only one amino acid residue (H272Y) from KPC-2, and their kinetic properties ( $K_m$  and  $k_{cat}$  values) towards  $\beta$ -lactams are rather similar. The active site of KPC enzymes includes, as other class A  $\beta$ -lactamases, several conserved elements which appear to be directly or indirectly involved in the substrate recognition and catalytic processes. The crystal structure of KPC-2 shows that this enzyme contains two subdomains one of which is  $\alpha$ -helical and the other subdomain contains five  $\beta$ -sheets [15]. The active site contains the catalytic residue S70 typical of all class A  $\beta$ -lactamases and some conserved residues such as K73, W105, N132, E166, R220 and K234. Residue E166 is involved in the deacylation step of catalysis; residues W105 and R220 are situated on the opposite sides of the active site and seem to be correlated with the recognition of substrates and inhibitors [16,17]. Several studies have been performed to state, in KPC enzymes, the role of active and non-active site residues [15–18]. In the present study, the role of a non-active site residue (D228) situated far from the catalytic “centre” of the KPC-3 enzyme was investigated. The molecular modelling of KPC-3 showed that residue 228 is positioned between  $\alpha$ 11 helix and  $\beta$ 7 sheet in the opposite side respect to the  $\Omega$ -loop and its side chain is exposed to the solvent (Figure 1). This study aims to answer a simple question: does a non-active residue, positioned far from the active site, influence substrate hydrolysis of KPC-3?

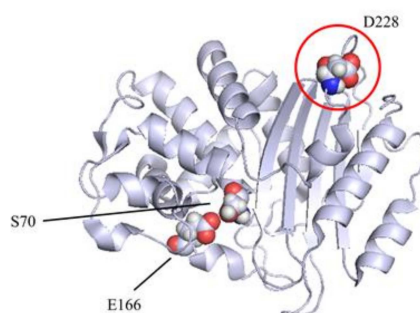


**Figure 1.** Ribbon representation of the KPC-3 enzyme. Molecular modelling was performed by PyMOL version 2.3 (PDB code: 6QWD).

## 2. Results

### 2.1. KPC-3 Mutants

Site-saturation mutagenesis, carried out on  $bla_{KPC-3}$ , has generated *E. coli* XL-1/ $bla_{D228X}$  recombinant strains which survived to ampicillin selection. Nevertheless, in the present study, only seven recombinant clones were chosen on the basis of their amino acid residue introduced at position 228. The seven D228X mutants analysed included residues with different chemical characteristics: neutral and nucleophilic small residues such as glycine and serine, respectively (D228G and D228S); an aromatic residue such as tryptophan (D228W); basic residue such as lysine (D228K); hydrophobic residues such as methionine, leucine and isoleucine (D228M, D228L and D228I).

### 2.2. Cloning and $\beta$ -Lactamase Purification

To overproduce KPC-3 and D228X enzymes, the  $bla_{KPC-3}$ ,  $bla_{D228S}$ ,  $bla_{D228W}$ ,  $bla_{D228M}$ ,  $bla_{D228K}$ ,  $bla_{D228L}$ ,  $bla_{D228I}$  and  $bla_{D228G}$  were sub-cloned into the pET-24a(+) vector and inserted by transformation in *E. coli* BL21(DE3). The purification protocol used permitted us to recover a total of 4 mg of each enzyme (purity higher than 95%).

### 2.3. Steady-State Kinetic Parameters

The KPC-3 and D228X pure enzymes were used for steady-state kinetic assays towards selected  $\beta$ -lactams, including benzylpenicillin, carbenicillin, cefotaxime, cefazolin, ceftazidime, imipenem, meropenem and ertapenem. The data obtained are displayed in Table 1.

**Penicillins.** All the enzymes, with the exception of D228G, hydrolysed benzylpenicillin better than carbenicillin (Table 1). Compared with KPC-3, D228X variants exhibited a decrease of  $k_{cat}$  and  $k_{cat}/K_m$  values for benzylpenicillin. Different behaviour was observed for carbenicillin:  $k_{cat}$  values of D228X variants were quite similar to that of KPC-3. Only D228G showed  $k_{cat}$  and  $k_{cat}/K_m$  values against carbenicillin 4-fold higher than KPC-3. Compared to KPC-3, the variants D228S, D228W, D228K, D228M, D228L and D228I showed an increase of  $K_m$  values for carbenicillin and, consequently, lower  $k_{cat}/K_m$  values.

**Table 1.** Kinetic parameters calculated for KPC-3 laboratory mutants towards some  $\beta$ -lactams.

Substrates ( $\beta$ -Lactams)		KPC-3	D228S	D228W	D228K	D228M	D228L	D228I	D228G
Benzylpenicillin	$K_m$ ( $\mu\text{M}$ )	144 $\pm$ 22	97 $\pm$ 8	187 $\pm$ 1	75 $\pm$ 5	248 $\pm$ 14	20 $\pm$ 2	25 $\pm$ 2	70 $\pm$ 6
	$k_{\text{cat}}$ ( $\text{s}^{-1}$ )	708 $\pm$ 15	48 $\pm$ 2	157 $\pm$ 4	136 $\pm$ 6	131 $\pm$ 5	37 $\pm$ 1	29 $\pm$ 1	35 $\pm$ 2
	$k_{\text{cat}}/K_m$ ( $\mu\text{M}^{-1} \text{s}^{-1}$ )	4.92	0.49	0.84	1.81	0.53	1.85	1.16	0.5
Carbenicillin	$K_m$ ( $\mu\text{M}$ )	108 $\pm$ 10	281 $\pm$ 12	179 $\pm$ 10	494 $\pm$ 18	240 $\pm$ 15	280 $\pm$ 30	182 $\pm$ 8	100 $\pm$ 5
	$k_{\text{cat}}$ ( $\text{s}^{-1}$ )	18 $\pm$ 1	17 $\pm$ 1	27 $\pm$ 1	36 $\pm$ 2	25 $\pm$ 2	14 $\pm$ 1	21 $\pm$ 2	70 $\pm$ 3
	$k_{\text{cat}}/K_m$ ( $\mu\text{M}^{-1} \text{s}^{-1}$ )	0.17	0.06	0.15	0.07	0.10	0.05	0.12	0.7
Cefotaxime	$K_m$ ( $\mu\text{M}$ )	57 $\pm$ 3	$\geq 1000$	373 $\pm$ 21	629 $\pm$ 50	238 $\pm$ 15	390 $\pm$ 28	430 $\pm$ 30	950 $\pm$ 48
	$k_{\text{cat}}$ ( $\text{s}^{-1}$ )	333 $\pm$ 12	N.D.	108 $\pm$ 5	68 $\pm$ 2	931 $\pm$ 21	34 $\pm$ 2	41 $\pm$ 2	244 $\pm$ 11
	$k_{\text{cat}}/K_m$ ( $\mu\text{M}^{-1} \text{s}^{-1}$ )	5.84	N.D.	0.29	0.11	3.91	0.09	0.09	0.21
Cefazolin	$K_m$ ( $\mu\text{M}$ )	189 $\pm$ 25	150 $\pm$ 8	119 $\pm$ 11	126 $\pm$ 14	141 $\pm$ 18	76 $\pm$ 6	121 $\pm$ 15	205 $\pm$ 17
	$k_{\text{cat}}$ ( $\text{s}^{-1}$ )	351 $\pm$ 9	11 $\pm$ 0.4	413 $\pm$ 3	644 $\pm$ 8	519 $\pm$ 14	64 $\pm$ 4	93 $\pm$ 4	271 $\pm$ 8
	$k_{\text{cat}}/K_m$ ( $\mu\text{M}^{-1} \text{s}^{-1}$ )	1.86	0.07	3.47	5.11	3.68	0.84	0.77	1.32
Ceftazidime	$K_m$ ( $\mu\text{M}$ )	100 $\pm$ 15	$> 1000$	400 $\pm$ 18	506 $\pm$ 25	300 $\pm$ 20	321 $\pm$ 38	960 $\pm$ 23	$> 1000$
	$k_{\text{cat}}$ ( $\text{s}^{-1}$ )	1.4 $\pm$ 0.1	N.D.	3.2 $\pm$ 0.1	1.8 $\pm$ 0.1	2.2 $\pm$ 0.1	0.5 $\pm$ 0.1	3.7 $\pm$ 0.5	N.D.
	$k_{\text{cat}}/K_m$ ( $\mu\text{M}^{-1} \text{s}^{-1}$ )	0.01	N.D.	0.01	0.004	0.007	0.002	0.004	N.D.
Imipenem	$K_m$ ( $\mu\text{M}$ )	88 $\pm$ 6	83 $\pm$ 4	128 $\pm$ 23	88 $\pm$ 5	87 $\pm$ 8	110 $\pm$ 10	104 $\pm$ 8	50 $\pm$ 2
	$k_{\text{cat}}$ ( $\text{s}^{-1}$ )	41 $\pm$ 2	34 $\pm$ 1	115 $\pm$ 9	116 $\pm$ 5	118 $\pm$ 2	19 $\pm$ 1.5	30 $\pm$ 1	26 $\pm$ 1
	$k_{\text{cat}}/K_m$ ( $\mu\text{M}^{-1} \text{s}^{-1}$ )	0.46	0.41	0.89	1.32	1.36	0.17	0.29	0.52
Meropenem	$K_m$ ( $\mu\text{M}$ )	68 $\pm$ 3	19 $\pm$ 2	46 $\pm$ 1	99 $\pm$ 5	48 $\pm$ 3	34 $\pm$ 1	62 $\pm$ 2	36 $\pm$ 1
	$k_{\text{cat}}$ ( $\text{s}^{-1}$ )	51 $\pm$ 2	3 $\pm$ 0.1	7 $\pm$ 0.3	8 $\pm$ 0.5	5 $\pm$ 0.3	4 $\pm$ 0.2	5 $\pm$ 0.1	11 $\pm$ 1
	$k_{\text{cat}}/K_m$ ( $\mu\text{M}^{-1} \text{s}^{-1}$ )	0.75	0.16	0.15	0.08	0.10	0.12	0.08	0.31
Ertapenem	$K_m$ ( $\mu\text{M}$ )	30 $\pm$ 1	63 $\pm$ 4	40 $\pm$ 3	26 $\pm$ 1	30 $\pm$ 2	21 $\pm$ 1	29 $\pm$ 2	18 $\pm$ 1
	$k_{\text{cat}}$ ( $\text{s}^{-1}$ )	5 $\pm$ 0.5	23 $\pm$ 2	25 $\pm$ 1	10 $\pm$ 1	82 $\pm$ 1	7 $\pm$ 0.4	11 $\pm$ 0.5	7 $\pm$ 0.2
	$k_{\text{cat}}/K_m$ ( $\mu\text{M}^{-1} \text{s}^{-1}$ )	0.17	0.37	0.62	0.38	2.73	0.33	0.38	0.39

**Carbapenems.** Regards carbapenems, KPC-3 and D228X variants showed different kinetic behaviour against imipenem, meropenem and ertapenem. Compared to KPC-3, all D228X variants displayed lower  $k_{\text{cat}}$  and  $k_{\text{cat}}/K_m$  against meropenem. Heterogeneity of  $k_{\text{cat}}$  values was observed for KPC-3 and D228X mutants against imipenem. Essentially, D228W, D228K and D228M showed  $k_{\text{cat}}$  values about 3-fold higher than KPC-3. The D228S, D228L, D228I and D228G hydrolysed imipenem less than KPC-3. Concerning ertapenem, D228M exhibited  $k_{\text{cat}}$  and  $k_{\text{cat}}/K_m$  about 16-fold higher than KPC-3. The same trend was observed for other D228X variants with  $k_{\text{cat}}$  and  $k_{\text{cat}}/K_m$  values slightly higher than KPC-3.

**Cephalosporins.** Compared to KPC-3, the D228X enzymes showed high  $K_m$  values against oxyimino cephalosporins (cefotaxime and ceftazidime). Cefotaxime was efficiently hydrolysed by KPC-3 and most of D228X variants (Table 1). Indeed, KPC-3 and D228M showed  $k_{\text{cat}}$  values towards cefotaxime of  $333 \text{ s}^{-1}$  and  $931 \text{ s}^{-1}$ , respectively. Cefotaxime was well hydrolysed by D228S, but it was impossible to calculate the  $k_{\text{cat}}$  value because of the high  $K_m$  value ( $>1000 \mu\text{M}$ ). The KPC-3 and D228X enzymes showed low  $k_{\text{cat}}$  values against ceftazidime. As a result of high  $K_m$  values, the catalytic efficiency ( $k_{\text{cat}}/K_m$ ) of KPC-3 and D228X mutants against both cefotaxime and ceftazidime was very low. Examining data obtained for cefazolin, we observed that cefazolin was well hydrolysed by all D228X variants. In particular, D228K, D228M and D228W showed high  $k_{\text{cat}}$  values equal to  $644 \text{ s}^{-1}$ ,  $519 \text{ s}^{-1}$  and  $413 \text{ s}^{-1}$ , respectively (Table 1). Only D228S showed a  $k_{\text{cat}}$  value 32-fold lower than KPC-3. Indeed, the  $K_m$  values were quite similar to that observed for the KPC-3 enzyme.

#### 2.4. Circular Dichroism

With KPC-3 and the seven D228X enzymes, possible conformational changes resulting from the mutation were estimated by CD spectroscopy in the Far-UV. Thus, comparison of the eight spectra showed no significant differences in either their shape or their relative magnitude (Figure 2), thus indicating that mutation at position 228 did not affect the secondary structural content of the D228X variants. The secondary structural content of the wild-type enzyme and three mutants was calculated and is given in Table 2. It is identical, within the error limit, for all proteins and is  $(34 \pm 3)\%$  helix,  $(18 \pm 2)\%$   $\beta$ -sheet and  $(48 \pm 3)\%$  other secondary structures. Structural data found in the PDB for KPC-2  $\beta$ -lactamase (PDB code: 2OV5) indicates that the protein consists of 42–44% helices and 16–17%  $\beta$ -sheets [15]. Despite a slightly greater helical content, these values are in good agreement with those calculated from the CD spectra.

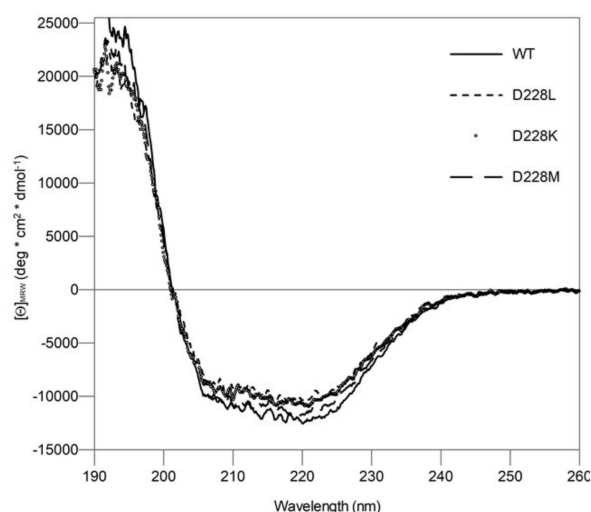


**Figure 2.** Far-UV CD spectra of KPC-3 and D228K, D228M and D228L mutants. Data were obtained at  $20 \text{ }^\circ\text{C}$ , in  $25 \text{ mM}$  sodium phosphate buffer,  $\text{pH } 7.0$ . Calculated secondary structural contents from these spectra are  $(34 \pm 3)\%$ ,  $(18 \pm 2)\%$ ,  $(19 \pm 1)\%$  and  $(29 \pm 2)\%$ , for  $\alpha$ -helices,  $\beta$ -strands, turns and unordered, respectively.

**Table 2.** Calculated secondary structures derived from the far-UV CD data.

Enzymes	Alpha	Beta	Turn	Unordered	Total	NRMSD <sup>(a)</sup>
KPC-3						
CDSSTR	39	17	18	26	100	0.055
CONTIN	36	16	19	29	100	0.036
SELCON	37	15	19	30	101	0.103
AVERAGE	37 ± 1.5	16 ± 1	18.7 ± 0.6	28 ± 2	100 ± 5	
D228L						
CDSSTR	33	21	19	27	100	0.061
CONTIN	29	20	20	30	99	0.049
SELCON	32	17	20	31	100	0.130
AVERAGE	31 ± 2	19 ± 2	19.7 ± 0.6	29 ± 2	100 ± 7	
D228K						
CDSSTR	34	18	19	28	99	0.059
CONTIN	31	17	20	31	99	0.043
SELCON	34	17	20	30	101	0.120
AVERAGE	33 ± 2	17.3 ± 0.6	19.7 ± 0.6	30 ± 1.5	100 ± 5	
D228M						
CDSSTR	37	18	18	27	100	0.055
CONTIN	34	18	19	30	101	0.046
SELCON	35	16	20	30	101	0.123
AVERAGE	35 ± 1.5	17.3 ± 1	19 ± 1	29 ± 2	100 ± 5	
GLOBAL AVERAGE	34 ± 3	18 ± 2	19 ± 1	29 ± 2	100 ± 8	

<sup>(a)</sup> Normalized Root Mean Square Deviations resulting from the analysis of the CD data with the CDPro software package.

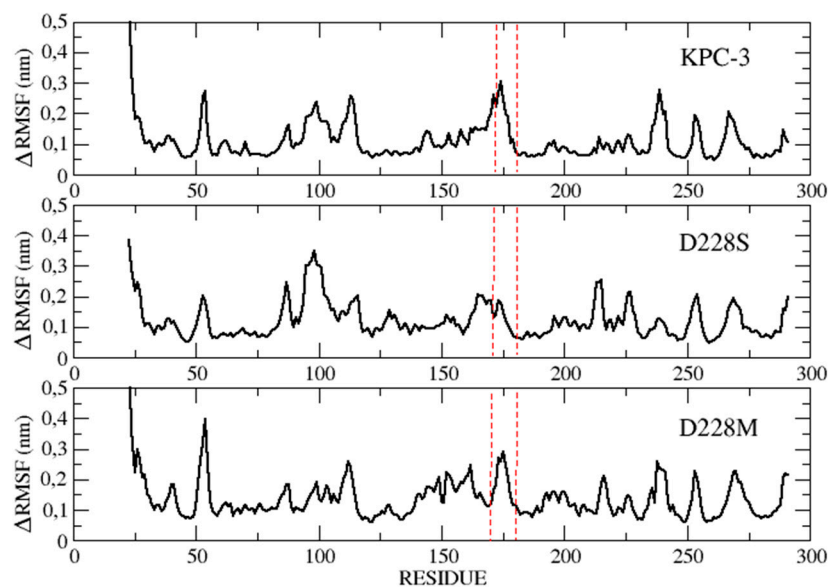
### 2.5. Fluorescence Assay

In addition to CD, fluorescence spectroscopy was used to analyse subtler structural changes among mutants and wild-type enzyme. Upon excitation at 280 nm, the intrinsic fluorescence of both KPC-3 and D228X variants exhibited similar fluorescence emission maximum around 350 nm. Nevertheless, some KPC-3 variants differed in fluorescence intensities. Compared with KPC-3 wild-type, the D228L mutant showed a 23% decrease in fluorescence intensity, whereas D228G and D228M exhibited increases in fluorescence intensity of 48% and 19%, respectively. Fluorescence intensity of D228I, D228S and D228K remained unchanged with respect to KPC-3.

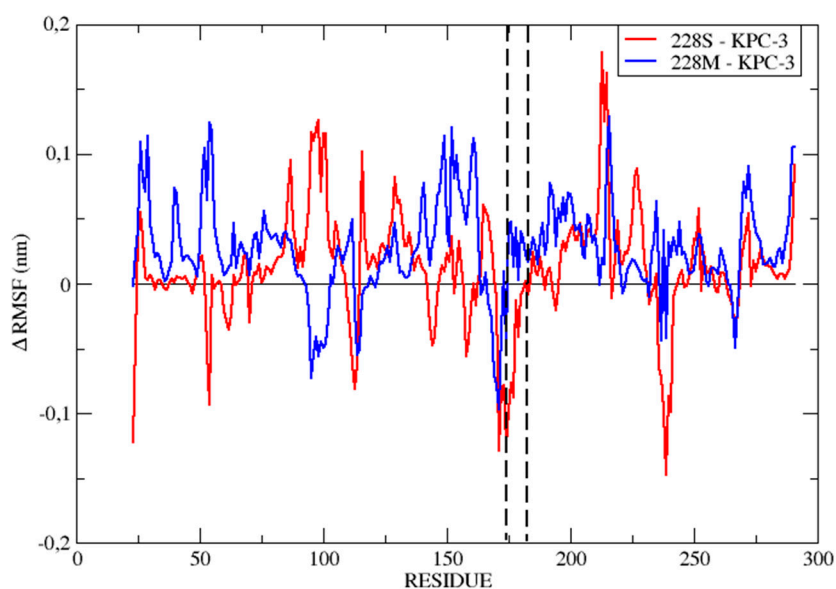
### 2.6. MD Simulations

To provide a qualitative rationalization of the kinetic data obtained, we decided to carry out MD simulations on D228S and D228M uncomplexed and complexed with cefotaxime. The D228S and D228M mutants showed  $K_m$  and  $k_{cat}$  values very different to KPC-3 wild-type. In our analysis (see figures), the same residue numbers of the crystal structure used as starting point of the simulation was used (PDB code: 6QWD). Figure 3A,B represent the C-alpha RMSF (Root Mean Square Fluctuation) of uncomplexed KPC-3, D228S and D228M. The uncomplexed KPC-3 is a rather stable structure, showing an overall RMSF much lower than the two uncomplexed mutants. Moreover, the fluctuation pattern observed in the three systems are sharply different hence indicating that a single mutation is, in principle, able of producing not significant dynamic differences. In D228S we can appreciate an increase and decrease of mobility of several regions. Indeed, fluctuation increase was observed in 93–106, 125–137, 164–168, 196–230, 248–256 and 264–267 regions, whereas fluctuation decrease was detected in 53–63, 109–115, 142–146, 157–161, 171–178, 235–242 regions. Specifically, D228S mutation induced a sharp decrease in the mobility of a large part of the  $\Omega$ -loop (171–178) and an increase of fluctuations in 196–230. This last region includes residue R220 that seems to be involved in the substrate recognition [15]. Differently to D228S, in D228M mutant an increase of fluctuations was observed in

the N-terminal (25–30, 39–43, 71–88) and also in 139–163, 175–202, 214–218, 233–245, 269–276 regions. The more stable regions in D228M were 92–102, 113–116, 167–175, 236–240 and 264–267. The D228M substitution has produced a general and widely distributed increase of the fluctuation with respect to the KPC-3.



(A)



(B)

**Figure 3.** (A) C-alpha Root Mean Square Fluctuation of the uncomplexed KPC-3, D228S and D228M, as obtained by 100 ns of simulations disregarding the first 6 ns, which were considered as equilibration. (B) Difference between the uncomplexed mutant and KPC-3 Root Mean Square Fluctuation using the data of Figure 3A. The dotted lines (in both panels) indicate the region corresponding to the  $\Omega$ -loop.



When the three enzymes (KPC-3, D228S and D228M) were complexed with cefotaxime, a different picture was observed (Figure 4). The KPC-3 complexed with cefotaxime was a very stable enzyme, an increase of fluctuation was observed only in the 267–283 region. Likewise KPC-3, the D228M mutant undergoes a general mechanical stabilization upon substrate insertion. On the other hand, in D228S complexed with cefotaxime, the fluctuations were distributed along different regions.

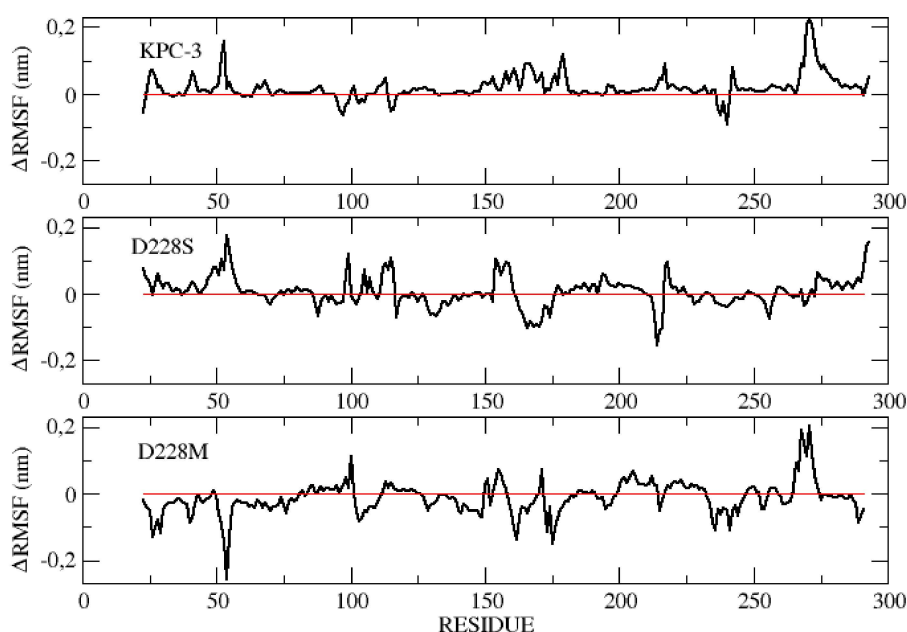


**Figure 4.** Difference between the complexed and uncomplexed Root Mean Square Fluctuation pattern in the three systems.

The uncomplexed KPC-3 is a rather stable structure showing an overall RMSF much lower than the two uncomplexed mutants (Table 3). The fluctuation pattern observed in the three systems are sharply different hence indicating that a single mutation is in principle able of producing not significant dynamic differences. On the other hand, it was almost impossible to relate the aforementioned results to the experimental kinetic observations. This is probably due to the huge number of plausible mechanical effects which could play some role in the enzyme activity. For this reason, we focused our attention on the effects localized in the active site. In particular, we monitored: (i) the distance between the substrate and the residues present in the active site; (ii) the inter-residues distances; and (iii) the presence of water molecules in specific positions known—or supposed—to have some importance in the acylation process. This latter analysis was accomplished by monitoring, at each frame, the simultaneous occurrence of H-bonds between one water molecule and two or more residues. We defined H-bond as any short-range contact according to the usual definition, i.e., Donor-Acceptor distance not higher than 0.35 nm and Donor-Hydrogen-Acceptor angle variation with respect to 180°, not exceeding 30°.

**Table 3.** Overall Root Mean Square Fluctuation (nm) of the six investigated species.

Specie	Uncomplexed Species	Complexed Species
KPC-3	29.1 nm	34.0 nm
D228S	32.2 nm	34.0 nm
D228M	36.2 nm	32.0 nm



From Figure 5 we observe that: (i) in general, the four residues S70, S130, K73 and K234 provide a stable (low standard deviation) framework of the complexed active site; (ii) as previously reported, in all the systems the substrate interacts quite tightly with S70, and S130. (iii) E166 appears as markedly flexible (high standard deviation) in the case of KPC-3 and stably far from the other residues (and the substrate) in the case of D228S. Moreover, E166, supposed to act as a base versus S70, is able to interact with the latter through a bridge water molecule (probably essential for the acid–base reaction) only in the KPC-3 and D228M enzymes. On the other hand, we could not find any appreciable presence E166-WAT-S70 bridge in D228S.

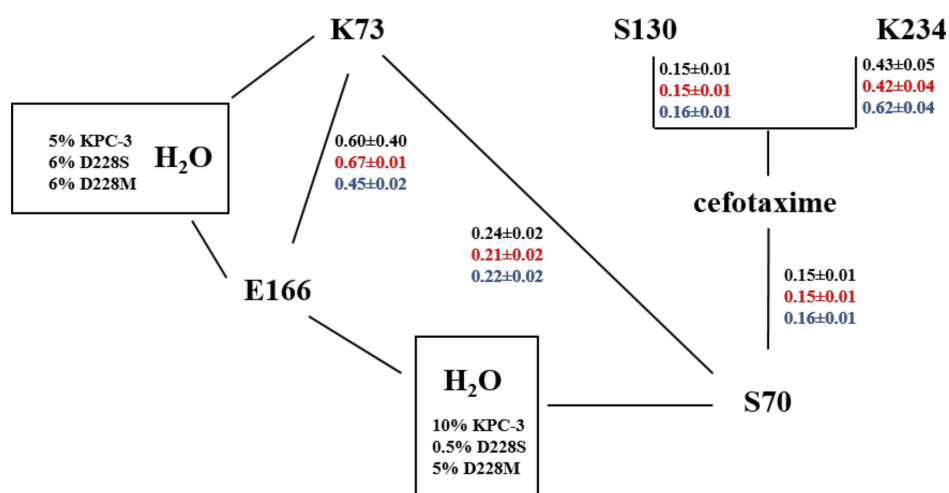


**Figure 5.** Average minimum distances and related standard deviations (in nm) between active-site residues and the Substrate. In black, red and blue we report the results for KPC-3, D228S and D228M, respectively. The ‘minimum distance’ indicates the smallest distance between all the couples of atoms between the interacting species. In the boxes, we also report the probability of finding one water molecule acting as a bridge between two different residues.

### 3. Discussion

In the present study, we paid attention to residue 228, which is located between  $\alpha 11$  and  $\beta 7$  sheet in the opposite site from the  $\Omega$ -loop, but far from the active site. Specifically, residue 228 in KPC-3 is located upstream of the  $\beta 7$  sheet, which includes the triad 234KTG. In class A  $\beta$ -lactamases, this element forms the opposite wall of the catalytic cavity, and some side chains of these residues could be involved in the substrate binding [19]. The KPC-3 carbapenemase is considered an important carbapenemase that is responsible for the widespread emergence of carbapenem-resistance in *K. pneumoniae* and other nosocomial pathogens in European countries [20]. The clinical relevance of KPC-type enzymes comes from their ability to hydrolyse a broad range of  $\beta$ -lactams, including penicillins, first-generation cephalosporins, cefotaxime and carbapenems. The kinetic characterization was performed on KPC-3 and on the following laboratory variants: D228S, D228W, D228K, D228M, D228L, D228I and D228G. Even if residue 228 is extremely unlikely to directly interact with the substrates, the kinetic parameters determined for the variants were significantly different from those measured with the wild-type enzyme. Since data obtained from CD analysis indicated that the mutation at position 228 does not affect the secondary structural content of the enzymes, fluorescence spectroscopy was performed to determine subtler structural differences. Fluorescence spectra are sensitive to the tryptophan environment, and its fluorescence is strongly affected by the polarity of the surroundings. All our enzymes, KPC-3 and D228X variants, showed a fluorescence maximum around 350 nm. Nevertheless, variations in fluorescence intensities observed in D228L, D228G and D228M allowed us to estimate changes in the microenvironment of aromatic fluorophores. These shifts could disclose changes in enzyme structure that led tryptophans to interact with different residues. To give a qualitative

rationalization of the observed kinetic data, we decided to carry out MD simulations. The simulations of KPC-3, D228S and D228M were performed complexed, with cefotaxime as substrate, and uncomplexed. In the uncomplexed systems, the KPC-3 enzyme was more stable than the two mutants. In D228S and D228M mutants, the replacement at position 228 generated a considerable number of fluctuations in several regions, making them less stable. The insertion of substrate (cefotaxime), which maintained a stable position in the active site throughout the simulation, clearly affected all of the mechanical features of the three systems (KPC-3, D228S and D228M) in a different fashion. In two of the above cases, we observed a general increase in fluctuation, either concentrated only in the 267–283 region (KPC-3) or distributed throughout different regions (D228S). The D228M enzyme seems more stable when complexed with cefotaxime and this behaviour could explain the higher value of  $k_{cat}$  for cefotaxime, but also for ceftazidime, than KPC-3. The increase of catalytic efficiency for ceftazidime has already been described for some natural KPC variants. As described by Mehta et al., a remarkable increase of resistance to ceftazidime was also observed in KPC-4 (P104R–V240G), KPC-8 (V240G–H274Y) and KPC-10 (P104R–H274Y) [18]. Increase in ceftazidime resistance is attributable to the substitutions at position 104 and 240. An interesting result in perfect agreement with kinetic data emerged when attention was directed towards the active site. Inside of the catalytic site, we noticed that one water molecule was (a) quite stable in KPC-3, (b) a little less stable in D228M, and (c) completely absent in D228S mutant. The last observation could explain the low affinity of the D228S variant for cefotaxime.

## 4. Materials and Methods

### 4.1. Cloning and Site-Saturation Mutagenesis

The  $bla_{KPC-3}$  gene was isolated by PCR from *K. pneumoniae* KP1/11 clinical isolate [21]. The  $bla_{KPC-3}$  gene was cloned into pBC-SK (+) vector using *KpnI* and *SacI* restriction sites. The pBC-SK/KPC-3 recombinant plasmid was inserted into *E. coli* XL-1 and used as a template to mutate, by site-saturation mutagenesis, the codon <sup>679</sup>GAC encoding for the 228 residue in KPC-3. Mutation was introduced into a PCR amplicon using mutagenic primers (KPC3D228\_F 5'-GTGCCGGCANNNTGGGCAGTC-3' and KPC3D228\_R 5'-GACTGCCCCANNNTGCCGGCAC-3') in combination with external primers (KPC\_F ATGTCAGTGTATCGCCGTCTAGTT and KPC\_R TTACTGCCCGTTGACGCCCAAT) by the overlap extension method, as reported in our previous paper [22]. Each fragment was sequenced three times using ABI PRISM 3500 automated sequencer (Life Technologies, Monza, Italy). The  $bla_{KPC-3}$  mutant genes were cloned into pBC-SK (+) vector. *E. coli* XL-1 competent cells were used as host for transformation experiments. The recombinant clones were selected on LB agar plates supplemented with chloramphenicol 30 mg/L and ampicillin 20 mg/L. Recombinant plasmids were sequenced to verify their authenticity. The  $bla_{KPC-3}$  and selected  $bla_{D228X}$  mutant genes were sub-cloned in pET-24a (+) vector using *NdeI* and *BamHI* restriction enzymes. *E. coli* NovaBlue strain was used as the non-expression host for the initial cloning, and the recombinant plasmids were then transferred into *E. coli* BL21(DE3) for enzyme expression.

### 4.2. Overexpression and Purification of KPC-3 and D228X Mutants

*E. coli* BL21 (DE3) cells carrying the recombinant plasmids pET24- $bla_{KPC-3}$  and pET24- $bla_{D228X}$  were grown in 2 L of LB medium with 50 mg/L kanamycin at 37 °C in an orbital shaker (180 rpm). The isopropyl-β-thiogalactoside (IPTG), at concentration of 0.4 mM, was added when the culture reached an absorbance of 0.7 at  $\lambda = 600$  nm. After addition of IPTG, the culture was incubated for 6 h at 22 °C under aerobic conditions. Cells were harvested by centrifugation at 8000 rpm for 10 min at 4 °C, washed twice with 25 mM sodium phosphate buffer (pH 7.0). The cells were then suspended in 30 mM Tris-HCl buffer (pH 8.0) containing 27% sucrose. The periplasm fraction was extracted by addition of lysozyme (final concentration, 0.4 mg/mL) and EDTA (final concentration, 5 mM) to the cooled solution. After 50 min of incubation on ice, the reaction was completed by adding MgSO<sub>4</sub> (final concentration, 5 mM). The sample was then centrifuged at 30,000 rpm for 30 min (4 °C). Supernatant was dialyzed overnight at 4 °C in

25 mM sodium acetate buffer (pH 5.2) and loaded onto a SP Sepharose FF equilibrated with the same buffer. The column was washed extensively to remove unbound proteins, and the  $\beta$ -lactamase was eluted with a linear gradient of NaCl (0 to 1 M) in the same buffer. Active fractions were pooled and dialyzed in 25 mM sodium phosphate buffer, pH 7.0, and loaded onto Sephacryl S-100 column (XK16/70, bed volume 130 mL) equilibrated with 25 mM sodium phosphate buffer (pH 7.0), 0.15 M NaCl. The active fractions were recovered and stored at  $-40\text{ }^{\circ}\text{C}$ .

#### 4.3. Determination of Kinetic Parameters

Kinetic experiments were performed following the hydrolysis of each substrate at  $25\text{ }^{\circ}\text{C}$  in 25 mM sodium phosphate buffer (pH 7.0). Data were collected with a Perkin-Elmer Lambda 25 spectrophotometer (Perkin-Elmer Italia, Milan, Italy). Steady-state kinetic experiments were performed under initial-rate conditions using the Hanes linearization method [23]. Each kinetic value is the mean of three different measurements; the error was below 10%.

#### 4.4. Fluorescence Emission Spectroscopy

Fluorescence studies were carried out on a Perkin-Elmer LS-50B spectrofluorometer (Perkin-Elmer Italia, Milan, Italy). The excitation wavelength was 280 nm and the emission spectra were recorded at  $25\text{ }^{\circ}\text{C}$ , in the range of 300–500 nm. The buffer used was 50 mM sodium phosphate buffer, pH 7.0. The concentration of each enzyme was 4 mg/L.

#### 4.5. Circular Dichroism

Far-UV CD spectra (190–260 nm) were recorded with a Jasco J-810 spectropolarimeter (Jasco, Tokyo, Japan) at  $20\text{ }^{\circ}\text{C}$  in 25 mM sodium phosphate, pH 7.0, using a 1 mm pathlength quartz Suprasil cell (Hellma), with protein concentrations of ca. 0.1 mg/mL. Five scans (20 nm/min, 0.1 nm bandwidth, 0.1 nm data pitch and 2 s DIT) were averaged, baselines were subtracted, and no smoothing was applied. Data are presented as the molar residue ellipticity ( $[\theta]_{\text{MRW}}$ ) calculated using the molar concentration of protein and number of residues. Secondary structure analyses using the CDSSTR, CONTINLL and SELCON3 programs were performed on the CD data with the CDPro software package, using a reference dataset SMP56 (i.e., IBasis 10) [24–29]. The results from the three algorithms were averaged, and the standard deviations were calculated.

#### 4.6. Molecular Dynamics (MD) Simulations

MD simulations were performed on KPC-3, D228S and D228M, uncomplexed and complexed with cefotaxime (substrate) using the Gromacs program [30]. For both enzymes and ligands, the Gromacs 54a7 force field and the Single Point Charge (spc) model were used for the solvent (water) [31]. For ligands, the atomic charge was calculated through Quantum Chemical calculations in the framework of Density Functional Theory using the hybrid Becke3LYP functional in conjunction with the 6-31G\* basis set and Gaussian 09 program [32,33]. All simulations were performed at 300 K using the LINCS and the Particle Mesh Ewald algorithms, in an isochoric/isothermal ensemble obtained with the velocity rescaling thermostat [34]. For all six simulations, we adopted the following protocol. The enzyme (uncomplexed and complexed) was located at the centre of the simulation box, filled with solvent molecules. After an initial energy minimization, the system was slowly heated up to 300 K using short (200.0 ps) runs. At 300 K the box dimension was adjusted in order to reproduce the same average pressure (1.0 atm) as that obtained by simulating a pure solvent box at the proper density at 298 K, as previously described [35]. The six simulations were extended for 100.0 ns. All the analyses were carried out excluding the first 6 ns from the whole trajectory, as these were considered to be equilibration. The KPC-3 initial structure was taken from the pdb file (code 6qwd.pdb). The same structure was also used in conjunction with the program MOLDEN for modelling the initial structure of D228S and D228M mutants [36]. Cefotaxime was modelled by adapting the crystal structure of the KPC-2  $\beta$ -lactamase complexed with the same hydrolysed substrate.

## 5. Conclusions

In the present paper, we demonstrated that amino acids replacement at position 228, which is far from catalytic site, causes important modification of KPC-3 activity against different  $\beta$ -lactams. The antibiotic resistance in Gram-negative bacteria represents a serious problem for the public health. The antibiotics actually used in clinical therapy are not enough to fight multi-drug resistant super bacteria, and new molecules need to be developed. In this context, our study identified a new possible target for molecules with inhibitory activity.

**Author Contributions:** Conceptualization, A.P. and M.P.; methodology, F.B., J.D.D., M.A., S.C., F.D.L. and A.M.; investigation, A.P.; data curation, A.P. and M.P.; writing—original draft preparation, A.P. and M.P.; writing—review and editing, A.P. and M.P.; supervision, M.P. and G.A.; project administration, M.P.; funding acquisition, M.P. and G.A. All authors have read and agreed to the published version of the manuscript.

**Funding:** This research was funded by CINECA—Italy, grant ISCRA-C.

**Acknowledgments:** The authors wish to thank Anna Toso (Toronto Catholic District School Board, Toronto, Canada) for the language revision of the manuscript.

**Conflicts of Interest:** The authors declare no conflict of interest.

## References

1. Bush, K.; Bradford, P.A. Epidemiology of  $\beta$ -lactamase-producing pathogens. *Clin. Microbiol. Rev.* **2020**, *33*, e00047-19. [[CrossRef](#)] [[PubMed](#)]
2. Tooke, C.L.; Hinchliffe, P.; Bragginton, E.C.; Colenso, C.K.; Hirvonen, V.H.A.; Takebayashi, Y.; Spencer, J.  $\beta$ -Lactamases and  $\beta$ -Lactamase Inhibitors in the 21st Century. *J. Mol. Biol.* **2019**, *431*, 3472–3500. [[CrossRef](#)] [[PubMed](#)]
3. Bush, K. Past and present perspectives on  $\beta$ -lactamases. *Antimicrob. Agents Chemother.* **2018**, *62*, e01076-18. [[CrossRef](#)] [[PubMed](#)]
4. Ambler, R.P. The structure of  $\beta$ -lactamases. *Philos. Trans. R. Soc. Lond. B Biol. Sci.* **1980**, *289*, 321–331.
5. Bush, K.; Jacoby, G.A. Updated functional classification of  $\beta$ -lactamases. *Antimicrob. Agents Chemother.* **2010**, *54*, 969–976. [[CrossRef](#)]
6. Garau, G.; García-Sáez, I.; Bebrone, C.; Anne, C.; Mercuri, P.; Galleni, M.; Frère, J.M.; Dideberg, O. Update of the standard numbering scheme for class B beta-lactamases. *Antimicrob. Agents Chemother.* **2004**, *48*, 2347–2349. [[CrossRef](#)]
7. Papp-Wallace, K.M.; Endimiani, A.; Taracila, M.A.; Bonomo, R.A. Carbapenems: Past, present, and future. *Antimicrob. Agents Chemother.* **2011**, *55*, 4943–4960. [[CrossRef](#)]
8. Palzkill, T. Structural and Mechanistic Basis for Extended-Spectrum Drug-Resistance Mutations in Altering the Specificity of TEM, CTX-M, and KPC  $\beta$ -lactamases. *Front. Mol. Biosci.* **2018**, *5*, 16. [[CrossRef](#)]
9. Naas, T.; Cuzon, G.; Villegas, M.V.; Lartigue, M.F.; Quinn, J.P.; Nordmann, P. Genetic structures at the origin of acquisition of the  $\beta$ -lactamase *bla*KPC gene. *Antimicrob. Agents Chemother.* **2008**, *52*, 1257–1263. [[CrossRef](#)]
10. Garcia-Fernandez, S.; Villa, L.; Carta, C.; Venditti, C.; Giordano, A.; Venditti, M.; Mancini, C.; Carattoli, A. *Klebsiella pneumoniae* ST258 producing KPC-3 identified in Italy carries novel plasmids and OmpK36/OmpK35 porin variants. *Antimicrob. Agents Chemother.* **2012**, *56*, 2143–2145. [[CrossRef](#)]
11. Pitout, J.D.; Nordmann, P.; Poirel, L. Carbapenemase-producing *Klebsiella pneumoniae*, a key pathogen set for global nosocomial dominance. *Antimicrob. Agents Chemother.* **2015**, *59*, 5873–5884. [[CrossRef](#)] [[PubMed](#)]
12. Chen, L.; Chavda, K.D.; Melano, R.G.; Jacobs, M.R.; Levi, M.H.; Bonomo, R.A.; Kreiswirth, B.N. Complete sequence of a *bla*(KPC-2)-harboring IncFII(K1) plasmid from a *Klebsiella pneumoniae* sequence type 258 strain. *Antimicrob. Agents Chemother.* **2013**, *57*, 1542–1545. [[CrossRef](#)] [[PubMed](#)]
13. Cerdeira, L.T.; Cunha, M.P.V.; Francisco, G.R.; Bueno, M.F.C.; Araujo, B.F.; Ribas, R.M.; Gontijo-Filho, P.P.; Knöbl, T.; de Oliveira Garcia, D.; Lincopan, N. IncX3 plasmid harboring a non-Tn4401 genetic element (NTE<sub>KPC</sub>) in a hospital-associated clone of KPC-2-producing *Klebsiella pneumoniae* ST340/CG258. *Diagn. Microbiol. Infect. Dis.* **2017**, *89*, 164–167. [[CrossRef](#)] [[PubMed](#)]

14. Alba, J.; Ishii, Y.; Thomson, K.; Moland, E.S.; Yamaguchi, K. Kinetics study of KPC-3, a plasmid-encoded class A carbapenem-hydrolyzing  $\beta$ -lactamase. *Antimicrob. Agents Chemother.* **2005**, *49*, 4760–4762. [[CrossRef](#)] [[PubMed](#)]
15. Ke, W.; Bethel, C.R.; Thomson, J.M.; Bonomo, R.A.; van den Akker, F. Crystal structure of KPC-2: Insights into carbapenemase activity in class A  $\beta$ -lactamases. *Biochemistry* **2007**, *46*, 5732–5740. [[CrossRef](#)]
16. Papp-Wallace, K.M.; Taracila, M.; Wallace, C.J.; Hujer, K.M.; Bethel, C.R.; Hornick, J.M.; Bonomo, R.A. Elucidating the role of Trp105 in the KPC-2  $\beta$ -lactamase. *Protein Sci.* **2010**, *19*, 1714–1727. [[CrossRef](#)]
17. Papp-Wallace, K.M.; Taracila, M.A.; Smith, K.M.; Xu, Y.; Bonomo, R.A. Understanding the molecular determinants of substrate and inhibitor specificities in the carbapenemase KPC-2: Exploring the roles of Arg220 and Glu276. *Antimicrob. Agents Chemother.* **2012**, *56*, 4428–4438. [[CrossRef](#)]
18. Mehta, S.G.; Rice, K.; Palzkill, T. Natural variants of the KPC-2 carbapenemase have evolved increased catalytic efficiency for ceftazidime hydrolysis at the cost of enzyme stability. *PLoS Pathog.* **2015**, *11*, e1004949. [[CrossRef](#)]
19. Matagne, A.; Lamotte-Brasseur, J.; Frère, J.M. Catalytic properties of class A  $\beta$ -lactamases: Efficiency and diversity. *Biochem. J.* **1998**, *330*, 581–598. [[CrossRef](#)]
20. Munoz-Price, L.S.; Poirel, L.; Bonomo, R.A.; Schwaber, M.J.; Daikos, G.L.; Cormican, M.; Cornaglia, G.; Garau, J.; Gniadkowski, M.; Hayden, M.K.; et al. Clinical epidemiology of the global expansion of *Klebsiella pneumoniae* carbapenemases. *Lancet Infect. Dis.* **2013**, *13*, 785–796. [[CrossRef](#)]
21. Perilli, M.; Bottoni, C.; Grimaldi, A.; Segatore, B.; Celenza, G.; Mariani, M.; Bellio, P.; Frascaria, P.; Amicosante, G. Carbapenem-resistant *Klebsiella pneumoniae* harbouring *bla*(KPC-3) and *bla*(VIM-2) from central Italy. *Diagn. Microbiol. Infect. Dis.* **2013**, *75*, 218–221. [[CrossRef](#)] [[PubMed](#)]
22. Piccirilli, A.; Mercuri, P.S.; Galleni, M.; Aschi, M.; Matagne, A.; Amicosante, G.; Perilli, M. P174E substitution in GES-1 and GES-5  $\beta$ -lactamases improves catalytic efficiency towards carbapenems. *Antimicrob. Agents Chemother.* **2018**, *62*, e01851-17. [[CrossRef](#)] [[PubMed](#)]
23. Segel, I.H. *Biochemical Calculations*, 2nd ed.; John Wiley & Sons: New York, NY, USA, 1976; pp. 236–241.
24. Manavalan, P.; Johnson, W.C., Jr. Variable selection method improves the prediction of protein secondary structure from circular dichroism spectra. *Anal. Biochem.* **1987**, *167*, 76–85. [[CrossRef](#)]
25. Sreerama, N.; Woody, R.W. Estimation of protein secondary structure from circular dichroism spectra: Comparison of CONTIN, SELCON, and CDSSTR methods with an expanded reference set. *Anal. Biochem.* **2000**, *287*, 252–260. [[CrossRef](#)]
26. Provencher, S.W.; Glöckner, J. Estimation of globular protein secondary structure from circular dichroism. *Biochemistry* **1981**, *20*, 33–37. [[CrossRef](#)]
27. Van Stokkum, I.H.; Spoelder, H.J.; Bloemendal, M.; van Grondelle, R.; Groen, F.C. Estimation of protein secondary structure and error analysis from circular dichroism spectra. *Anal. Biochem.* **1990**, *191*, 110–118. [[CrossRef](#)]
28. Sreerama, N.; Woody, R.W. A self-consistent method for the analysis of protein secondary structure from circular dichroism. *Anal. Biochem.* **1993**, *209*, 32–44. [[CrossRef](#)]
29. Sreerama, N.; Venyaminov, S.Y.; Woody, R.W. Estimation of the number of alpha-helical and beta-strand segments in proteins using circular dichroism spectroscopy. *Protein Sci.* **1999**, *8*, 370–380. [[CrossRef](#)]
30. Van Der Spoel, D.; Lindahl, E.; Hess, B.; Groenhof, G.; Mark, A.E.; Berendsen, H.J.C. GROMACS: Fast, flexible, and free. *J. Comput. Chem.* **2005**, *26*, 1701. [[CrossRef](#)]
31. Schmid, N.; Eichenberger, A.P.; Choutko, A.; Riniker, S.; Winger, M.; Mark, A.E.; van Gunsteren, W.F. Definition and testing of the GROMOS force-field versions 54A7 and 54B7. *Eur. Biophys. J.* **2011**, *40*, 843–856. [[CrossRef](#)]
32. Becke, A.D. A new mixing of Hartree-Fock and local density-functional theories. *J. Chem. Phys.* **1993**, *98*, 1372–1377. [[CrossRef](#)]
33. Frisch, M.J.; Trucks, G.W.; Schlegel, H.B.; Scuseria, G.E.; Robb, M.A.; Cheeseman, J.R.; Scalmani, G.; Barone, V.; Mennucci, B.; Petersson, G.A.; et al. *Gaussian 09*; Revision E.01; Gaussian Inc.: Wallingford, CT, USA, 2013.
34. Piccirilli, A.; Brisdelli, F.; Aschi, M.; Celenza, G.; Amicosante, G.; Perilli, M. Kinetic Profile and Molecular Dynamic Studies Show that Y229W Substitution in an NDM-1/L209F Variant Restores the Hydrolytic Activity of the Enzyme toward Penicillins, Cephalosporins, and Carbapenems. *Antimicrob. Agents Chemother.* **2019**, *63*, e02270-18. [[CrossRef](#)] [[PubMed](#)]



35. Aschi, M.; D'Abramo, M.; Amadei, A. Photoinduced Electron Transfer in a Dichromophoric Peptide: A numerical experiment. *Theor. Chem. Acc.* **2016**, *135*, 132–142. [[CrossRef](#)]
36. Schaftenaar, G.; Noordik, J.H. Molden: A pre- and post-processing program for molecular and electronic structures. *J. Comput.-Aided Mol. Des.* **2000**, *14*, 123–134. [[CrossRef](#)] [[PubMed](#)]

**Publisher's Note:** MDPI stays neutral with regard to jurisdictional claims in published maps and institutional affiliations.



© 2020 by the authors. Licensee MDPI, Basel, Switzerland. This article is an open access article distributed under the terms and conditions of the Creative Commons Attribution (CC BY) license (<http://creativecommons.org/licenses/by/4.0/>).